Cloud inhomogeneity from MODIS

Lazaros Oreopoulos[1,2] and Robert F. Cahalan[2]

1. JCET-University of Maryland Baltimore County, Baltimore MD

2. Laboratory for Atmospheres, NASA-Goddard Space Flight Cente, Greenbelt, MD

Revised for J. Climate, May 2005

Corresponding author: Lazaros Oreopoulos, NASA GSFC, Code 613.2, Greenbelt, MD, 20771 USA. lazaros@climate.gsfc.nasa.gov, (301) 614-6128.

Abstract

Two full months (July 2003 and January 2004) of MODIS Atmosphere Level-3 data from the Terra and Aqua satellites are analyzed in order to characterize the horizontal variability of vertically integrated cloud optical thickness ("cloud inhomogeneity") at global scales. The monthly climatology of cloud inhomogeneity is expressed in terms of standard parameters, initially calculated for each day of the month at spatial scales of 1°x1°, and subsequently averaged at monthly, zonal, and global scales. Geographical, diurnal, and seasonal changes of inhomogeneity parameters are examined separately for liquid and ice phases, and separately over land and ocean. We find that cloud inhomogeneity is overall weaker in summer than in winter. For liquid clouds, it is also consistently weaker for local morning than local afternoon and over land than ocean. Cloud inhomogeneity is comparable for liquid and ice clouds on a global scale, but with stronger spatial and temporal variations for the ice phase, and exhibits an average tendency to be weaker for near overcast or overcast gridpoints of both phases. Depending on cloud phase, hemisphere, surface type, season, and time of day, hemispheric means of the inhomogeneity parameter ν (roughly the square of the ratio of optical thickness mean to standard deviation), have a wide range of ~1.7 to 4, while for the inhomogeneity parameter χ (the ratio of the logarithmic to linear mean) from ~0.65 to 0.8. Our results demonstrate that the MODIS Level-3 dataset is suitable for studying various aspects of cloud inhomogeneity and may prove invaluable for validating future cloud schemes in large scale models capable of predicting subgrid variability.

1. Introduction

The non-linear interplay of solar and longwave radiation with cloud optical properties is a fundamental aspect of atmospheric radiative transfer with implications for the Earth's climate that were already noted many years ago (e.g., Harshvardhan and Randall, 1985). In recent years, a plethora of studies examined various aspects of this interplay, but to our knowledge, only a handful was of global scope, namely the observational study of Rossow et al. (2002) and the model-based studies of Oreopoulos et al. (2004) and Räisänen et al. (2004). The present study, focusing only on a specific aspect of cloud variability, namely the horizontal fluctuations of total optical thickness τ (hereafter "cloud inhomogeneity") is also of global scope. Studies on this topic preceding Rossow et al. (2002) (hereafter RDC) provided an incomplete and often conflicting picture of the magnitude of cloud inhomogeneity as they were based on a limited number of scenes and different observational methods (Cahalan et al. 1994; Cahalan et al., 1995; Barker, 1996; Oreopoulos and Davies, 1998a; Pincus et al., 1999). In the following we make the case that, similar to the International Satellite Cloud Climatology Project (ISCCP) products used by RDC, higher level cloud products from the Moderate Resolution Imaging Spectroradiometer (MODIS) instrument aboard the Terra and Aqua satellites can provide a detailed picture of cloud inhomogeneity.

Knowledge of the actual geographical and seasonal distribution of cloud inhomogeneity is essential in our effort to make it a diagnosed or predicted quantity that will improve representation of physical processes involving clouds in Large Scale Models (LSMs). These include both cloud formation and precipitation processes (e.g., Jakob and Klein, 1999), but also radiative processes at solar and thermal wavelengths.

The need to improve radiative processes arises from the fact that plane-parallel homogeneous (PPH) radiation flux calculations, i.e., calculations where only the mean cloud optical properties of the gridbox are used, often exhibit significant errors compared to Independent Column Approximation (ICA) calculations where averages of plane parallel calculations on individual cloudy columns (currently not explicitly resolved by LSMs) or integrals over the probability density function (PDF) of optical properties are calculated. These systematic errors, frequently referred to as plane parallel biases (Cahalan et al., 1994), stem from the nonlinear dependence of both shortwave (SW) and longwave (LW) fluxes on cloud optical properties. The magnitude of the errors depends on solar geometry (for SW), the average amount of cloud water, cloud vertical overlap, and the degree of cloud variability. The SW albedo error, for example, was found from theoretical and observational studies to have a range of 0.025 to 0.3 (according to the survey of relevant literature by RDC), suggesting a very substantial impact on the energy budget. LSM modelers would not want their efforts to simulate correct mean distributions of cloud properties be hampered by their inability to produce realistic radiation budgets. If the goal is to develop schemes that account either implicitly or explicitly for cloud inhomogeneity (e.g. Tompkins, 2002), it is only logical to assume that descriptions of its magnitude from global observations will aid the development of the relevant algorithms.

Our paper provides important elements of this global description. It complements and expands RDC's study in a number of ways: it uses different inhomogeneity parameters calculated at different spatial scales and applies for clouds that are classified in a different manner and whose properties are retrieved at different spatial resolution, and aggregated in different ways. It is organized as follows: First, we present in section 2

the various parameters that have in recent years been used as descriptors of cloud inhomogeneity. Then in section 3 we discuss which of these parameters can be obtained from the MODIS dataset and under what limitations, and how they are averaged at various temporal and spatial scales. Section 4 is the centerpiece of the paper and discusses cloud variability features such as differences between clouds of liquid and ice phase, morning and afternoon clouds, marine and continental clouds, winter and summer clouds, and relationships with cloud fraction. A summary of the findings, and their potential uses is offered in the final section.

2. Measures of cloud inhomogeneity

A short overview of the various parameters that have been used to quantify cloud inhomogeneity is provided below. Comparisons among the various horizontal inhomogeneity parameters provide insight on the features of the optical property distribution from which they were derived (see the excellent discussion by RDC).

The inhomogeneity parameter χ first introduced by Cahalan et al. (1994) is defined as the ratio of the logarithmic and linear average of a cloud optical thickness distribution:

$$\chi = \frac{e^{\overline{\ln \tau}}}{\overline{\tau}} \qquad 0 < \chi \leq 1 \qquad (1)$$

with

$$\overline{\tau} = \int \tau p(\tau) \mathrm{d}(\tau) \qquad (2)$$

and $\overline{\ln \tau}$ defined similarly:

$$\overline{\ln \tau} = \int \ln \tau p(\tau) \mathrm{d}\tau \qquad (3)$$

$p(\tau)$ is the PDF of cloud optical thickness τ. The inception of χ was inspired by the fact that the reflected solar flux is a linear function of the logarithm of optical thickness for a wide range (~5 to ~30, depending on solar zenith angle–SZA) of optical thicknesses. Thus, the "effective" optical thickness $\chi\bar{\tau}$ is the logarithmically averaged optical thickness and generally provides a better regional albedo estimate than $\bar{\tau}$ when used as input in plane-parallel radiative transfer calculations (this is known as ETA–Effective Thickness Approximation). Oreopoulos and Davies (1998b) compared χ to χ_0:

$$\chi_0 = \frac{\hat{\tau}}{\bar{\tau}} = \frac{\mathbf{R}^{-1}(R_{\mathrm{ICA}})}{\bar{\tau}} \qquad 0 < \chi_0 \le 1 \qquad (4)$$

i.e., the ratio of the radiatively averaged optical thickness (the optical thickness that corresponds to the average reflectance $-R_{\mathrm{ICA}}-$ of a region, possibly also integrated over the SZA) to the linearly averaged optical thickness. The inhomogeneity parameter ε used by RDC to express the ISCCP cloud inhomogeneity climatology is simply $1-\chi_0$. Note that derivation of χ_0 from MODIS requires forward radiative transfer calculations to obtain R_{ICA}, and no results for this parameter are shown here.

A different class of cloud horizontal inhomogeneity measures is related to theoretical distributions that have been found to be good fits of observed PDFs of τ (Barker, 1996). For example, ν, the shape parameter of a gamma distribution, can be derived from the ratio of mean to standard deviation (σ_τ) of the distribution, in which case it is said that it is derived from the Method of Moments (MOM):

$$\nu_{MOM} = \left(\frac{\bar{\tau}}{\sigma_\tau} \right)^2 \tag{5}$$

Within the context of the gamma distribution, ν can also be estimated from the Maximum Likelihood Estimate (MLE) method (Wilks, 1995) which is less sensitive to outliers than MOM (Oreopoulos and Davies 1998b) and can be approximated by (Wilks, 1995):

$$\nu_{MLE} = \frac{1 + \sqrt{1 + 4y/3}}{4y} \tag{6a}$$

$$y = \ln \bar{\tau} - \overline{\ln \tau} \tag{6b}$$

The parameter ν (of both the MOM and MLE variety) can in principle also be inferred from satellite observations, and therefore from MODIS as well (as explained in the next section). Eqs. (1)-(6) are often also applied to PDFs of cloud water path (W).

The various parameters defined above have their own advantages and disadvantages as descriptors of cloud inhomogeneity, and when intercompared can reveal properties of the PDF from which they were derived. For example, large deviations of χ from χ_0 are

encountered for PDFs that are very wide, e.g., consisting of few very thick convective clouds mixed with very thin cirrus clouds as is common in the Tropics (RDC); large discrepancies between ν from MOM and MLE is indicative of ill-behaved PDFs, e.g., distributions with a small number of extremely large τ values that produce too small MOM values of ν for the resulting gamma distribution to be a good fit. In general, as RDC pointed out, the problem with inhomogeneity measures that involve calculations of the second moment of the PDF is that there may be convergence problems in the case of highly skewed or multimodal PDFs and in situations of limited sample population (e.g., from PDFs derived from a single snapshot in regions with low cloud cover). Additional criteria explained below made χ the primary focus of this study, while ν_{MOM} is the inhomogeneity parameter receiving the least attention.

3. The MODIS dataset

a. Analysis method

For the analysis in this paper we rely on Level-3 (L-3) (Global Gridded) MODIS cloud products. These products describe the physical and radiative properties of clouds including cloud particle phase (ice vs. liquid water), effective cloud particle radius, cloud optical thickness, cloud top temperature, cloud top height, effective emissivity, and cloud fraction under both daytime and nighttime conditions (Platnick et al., 2003). There are three L-3 MODIS cloud products for daily (D3), eight-day (E3), and monthly (M3) time periods, collected from two platforms, Terra and Aqua. Each L-3 product contains statistics for various cloud parameters (also called Scientific DataSets or SDSs) generated from the Level-2 (L-2) (Orbital Swath) products. Statistics are summarized over a 1°x1°

global grid (King et al., 2003). In this study we only use D3 data, from which we extract the following SDSs (separately for the liquid and ice particle phases): mean, standard deviation and mean logarithm of τ, mean and standard deviation of W, histograms of τ and W, and mean (daytime) cloud fraction corresponding to successful cloud optical property retrievals.

All these statistics are computed by subsampling pixel-level (L-2) values every 5th pixel along both spatial directions (King et al., 2003). Thus, the cloud statistics for an overcast 1°x1° gridpoint around the equator come from about ~480 pixels instead of the ~12000 1-km pixels that originally fall within the gridpoint. Oreopoulos (2005) found that temporal (e.g., monthly) and/or spatial (e.g. zonal) averaging suppresses significantly the subsampling errors of χ and ν. For example, the percentage errors of monthly averages of individual gridpoints are usually below 10% for ν_{MOM} and ν_{MLE}. Errors for χ are even smaller (< 2%), and errors for all inhomogeneity parameters drop much further when zonal averages are taken.

Two months (July 2003 and January 2004) of D3 data for both the Terra and Aqua platforms are analyzed. The data come in Hierarchical Data Format (HDF) files separately for each day of the month, and are freely available worldwide from the NASA-Goddard Distributed Active Archive Center (DAAC) at http://daac.gsfc.nasa.gov.

Cloud inhomogeneity from MODIS D3 data can be estimated in several ways. First, the inhomogeneity parameters χ, ν_{MOM} and ν_{MLE} can be calculated from either W or τ statistics. Second, the moments used in eq. (1), (5), (6) (or their counterparts for W) can be derived either from histograms or directly obtained as distinct SDSs (in the case of $\overline{\ln W}$ only the histogram route is available). Third, one may wish to restrict the

presentation of the results to only one parameter. We chose to focus on the inhomogeneity parameter χ derived from moment SDSs of τ for the reasons given below, but ν_{MLE} values are still provided for the global and hemispheric results.

We opted to concentrate on inhomogeneity parameter results derived from SDSs of τ because it is the optical property directly retrieved from MODIS observations and the quantity that ultimately matters when estimating the radiative impact of cloud inhomogeneity. W on the other hand is derived by combining τ and effective radius (r_{eff}) retrievals and is by itself not sufficient for radiative calculations. We recognize that this choice may make validation of LSMs with this dataset somewhat more involved because in models it is W that is the fundamental quantity and τ is the by-product.

The inhomogeneity parameter findings presented in the following (except where noted otherwise) are calculated from eq. (1), (5), (6) using the appropriate distinct SDS moments. We chose this path of calculation because the SDS moments are derived directly from the L-2 data and are therefore more accurate than those calculated from the histograms which are subject to bin discretization errors, especially for second order moments or when cloud fractions are small. This way we also avoid interference of histogram discretization effects in the inhomogeneity parameter comparisons between the two phases (liquid and ice phase histograms have different discretizations).

There are several reasons why χ was given principal focus in this work. First, it suffers the least from L-3 subsampling as noted above. Second, because it is bounded by an upper value of 1 it can be more easily averaged than ν_{MOM} and ν_{MLE} which are unbounded (in the relatively few cases where individual gridpoint values of ν exceed 10,

their values were set back to 10 before temporal and spatial averaging). Third, χ is more physically intuitive as it represents the factor by which $\bar{\tau}$ should be scaled to approximate the regional albedo, and can thus be more directly compared to ε of RDC. For those prefering inhomogeneity expressed in terms of ν, we include ν values (mainly ν_{MLE}) in the presentation of global-scale results (Tables 1 and 3) and provide a table (Table 2) to help convert monthly zonal values of χ to monthly zonal values of ν.

The inhomogeneity measures obtained from the MODIS D3 dataset convey information mainly on spatial cloud variability since most regions are viewed only once by each satellite during daylight hours (this is less true for high latitudes where significant orbit overlap takes place). Spatial cloud inhomogeneity is of greater interest in this study than temporal variability because it is exactly the type we seek to advance in global modeling applications: layer cloud optical thickness varies with time in today's LSMs, but spatial (subgrid) variations at specific time steps are not produced. For the purposes of a cloud inhomogeneity climatology, the relevant quantities are the mean monthly values of inhomogeneity parameters derived by averaging the daily values.

The following equations are written for χ, but also apply for ν and are applied for each cloud phase (liquid/ice) separately. Only gridpoints for which the cloud fraction of the respective phase was greater than 0.1 and for which calculation of all three inhomogeneity parameters was possible (this implies that $\sigma_\tau > 0$ and $y > 0$) were used. Gridpoints not satisfying these conditions were either homogeneous (case $\sigma_\tau = 0$) or contained other ill-behaved PDFs.

For a 1°x1° region (m,n) in the mth meridional and nth latitudinal zone, the mean monthly value of the variability parameter χ is given by:

$$\hat{\chi}^C(m,n) = \frac{\sum_{l=1}^{L} C_l(m,n)\chi_l(m,n)}{\sum_{l=1}^{L} C_l(m,n)} \qquad (7)$$

where $C_l(m,n)$ is the cloud fraction for day l (also a D3 SDS given separately for each phase) and region (m,n), L is the number of days for which $C_l(m,n) > 0.1$ and calculation of all three inhomogeneity parameters was possible. Eq. (7) gives thus a weighted monthly mean value for a single gridpoint of the inhomogeneity parameter χ.

Zonal monthly averages of χ can be calculated using the values from eq. (7):

$$\left\langle \chi^C(n) \right\rangle = \frac{\sum_{m=1}^{M} \hat{C}(m,n)\hat{\chi}^C(m,n)}{\sum_{m=1}^{M} \hat{C}(m,n)} \qquad (8)$$

M is the number of 1°x1° gridpoints in a specific latitude zone n for which all three inhomogeneity parameters are available, and $\hat{C}(m,n) = \sum_{l=1}^{L} C_l(m,n)/L$ is the monthly averaged cloud fraction for those gridpoints. Global averages can be obtained for a single day or an entire month. For a single day:

$$\tilde{\chi}_l^C = \frac{\sum_{n=1}^{N}\sum_{m=1}^{M} w(n)C_l(m,n)\chi_l(m,n)}{\sum_{n=1}^{N}\sum_{m=1}^{M} w(n)C_l(m,n)} \tag{9}$$

where $w(n)=\cos[\mathrm{lat}(n)]$ is the weight for each latitude zone calculated as the cosine at the center of the latitude zone, and N is the number of latitude zones. The monthly global averages are obtained from:

$$\left[\chi^C\right] = \frac{\sum_{n=1}^{N}\sum_{m=1}^{M} w(n)\hat{C}(m,n)\hat{\chi}^C(m,n)}{\sum_{n=1}^{N}\sum_{m=1}^{M} w(n)\hat{C}(m,n)} \tag{10}$$

Eqs. (9) and (10) can also be used for hemispheric averages by appropriately setting the range of n values. Note that the cloud fraction $C_l(m,n)$ used in eq. (7) and (9) is not the cloud fraction of the MODIS cloud mask algorithm, but rather the cloud fraction corresponding to the number of pixels for which successful retrievals of cloud optical properties were completed. This cloud fraction is somewhat lower than the cloud fraction from the mask algorithm since it does not include pixels for which observed and pre-calculated radiances could not be matched for any vector of cloud properties.

b. MODIS limitations

MODIS can "see" only the total (integrated) optical thickness of one or more cloudy layers. A Column Radiation Model of an LSM capable of handling inhomogeneous clouds, on the other hand, would probably require the vertical profile of horizontal cloud variability. This cannot be provided by MODIS (which is not even providing the vertical

profile of $\bar{\tau}$). In the Tropics, for example, highly variable convective towers may be covered by thick but relatively homogeneous cirrus anvils and there would be no way for MODIS to untangle the inhomogeneity of the convective cloud. Another issue is "real" vs. "apparent" cloud inhomogeneity due to 3D radiative transfer effects present in MODIS observations. In the mid-latitudes, for instance, storm system clouds may look more inhomogeneous than they really are due to shadowing and side illumination effects not accounted for by the plane-parallel retrievals (Oreopoulos et al., 2000). In the first case, MODIS may underestimate the variability of convective clouds, in the second case, it may overestimate the variability of stratiform clouds. The systematic expressions of these MODIS limitations may actually aid the study of cloud inhomogeneity: the presence of 3D effects in cloud retrievals, and their apparent contributions to cloud inhomogeneity, may potentially be assessed from intercomparison among regions with climatologically similar single-layer clouds, but observed under different illumination conditions. Such issues will be given proper attention in a future study. Finally, we note that our analysis does not distinguish between inhomogeneity due to top height variations of clouds with relatively weak variations of extinction and inhomogeneity due to extinction variations of clouds with weakly varying top heights.

4. MODIS inhomogeneity climatology

a. Inhomogeneity parameter comparison and dependence on method of calculation

We start the analysis of inhomogeneity by discussing the sensitivity of global values of inhomogeneity parameters to the choice of calculation method (i.e., SDS moment-based vs. SDS histogram-based, as discussed previously).

Table 1 shows $\left[\chi^C\right]$, $\left[\nu_{MLE}^C\right]$, and $\left[\nu_{MOM}^C\right]$ for liquid and ice clouds from moment-based (index "1") and histogram-based (index "2") estimates. These are values from the Terra platform for July '03 and are calculated using eq. (10) (and its exact counterparts for ν_{MOM} and ν_{MLE}). Both τ and W-based estimates are provided. Also provided are estimates based on "QA" (Quality Assurance) SDS moments, i.e., moments calculated using the QA quality flags (Platnick et al., 2003) as weight. The results of Table 1 indicate that the moment-based and histogram-based methods give very similar global results for τ with only a slight tendency for smaller values (larger inhomogeneity) for the histogram-based method. The difference in ν_{MOM} between the two methods is a bit more pronounced for W whose histogram discretization is poorer than that of τ. On the other hand, use of QA-weighted statistics (only moments are available, not histograms) seems to have a greater impact, with global cloud inhomogeneity decreasing significantly (parameter values increasing). This is because lower weight is assigned to dubious retrievals which likely fall close to the extrema of the allowed range of assumed τ values. Since the results shown in the remainder of the paper are not based on QA-weighted statistics, it is conceivable that we overestimate cloud heterogeneity to some extent.

Considering that all monthly zonal inhomogeneity results that follow are expressed in terms of χ, it would be useful to have an empirical relationship to convert values of any one of the three inhomogeneity parameters χ, ν_{MOM} and ν_{MLE} to values of the other two. The relationships between χ and the ν's are in general different from gridpoint to gridpoint since they depend on PDF details, but we found that for zonal averages they can be approximated well by exponential functions. Table 2 summarizes the conversion rules

from $\langle \chi^C \rangle$ to $\langle \nu^C_{MLE} \rangle$ and $\langle \nu^C_{MOM} \rangle$ based on these exponential fits. The fits are of lower quality for high values of $\langle \chi^C \rangle$ where they can lead to $\langle \nu^C_{MOM} \rangle$ values that are higher than $\langle \nu^C_{MLE} \rangle$ (the opposite is usually true).

Figure 1 shows $\langle \chi^C(n) \rangle$ from eq. (8) for July'03/Jan'04 Terra liquid and ice clouds for both τ-based and W-based values, obtained from the histogram SDSs. In certain latitude zones particle size variations tend to reduce variability of liquid clouds (as in Räisänen et al., 2003) and increase variability of ice clouds. The differences are stronger at low latitudes and somewhat stronger in January for liquid clouds and in July for ice clouds. Still, extended regions of agreement between the two estimates can be seen in the midlatitudes, for both phases. On a global basis (Table 1), the values of $\lceil \chi^C \rceil$ indicate that liquid clouds are slightly less homogeneous for W-based estimates while the opposite is observed for ice clouds, but differences are quite small. This result is confirmed by the $\lceil \nu^C_{MLE} \rceil$ values for liquid clouds, but not those for ice clouds which are about the same. In the case of ν_{MOM}, where W-based estimates are possible from both the SDS moments and the W histograms the results depend on the method of calculation and are inconclusive.

All in all, r_{eff} variations do not appear to cause dramatic changes to the values of the inhomogeneity parameters on a global scale although they have some impact at smaller scales. This may be because the variability of r_{eff} is limited by the fact that particle size retrievals depend mostly on the cloud microphysical state near the cloud top (e.g., Platnick, 2000). Since W is not retrieved directly, but is the by-product of combining τ

and r_{eff} retrievals, we henceforth concentrate on inhomogeneity parameters inferred from τ distributions only.

b. Inhomogeneity of liquid clouds vs. inhomogeneity of ice clouds

The possible outcomes of the MODIS cloud thermodynamic phase identification algorithm are "uncertain phase", "mixed phase", "ice" or "liquid water" (Platnick et al., 2003). In this subsection we focus on the differences in inhomogeneity between the two "unambiguously" defined thermodynamic phases, i.e., "ice" and "liquid" water. For thick clouds, phase determination is sensitive to the cloud state near its top. Clouds with strong vertical development will be classified as ice clouds due to their low brightness temperature even if they consist of liquid droplets at lower levels. By the same token, pixels where relatively thick ice clouds overlie lower-level liquid clouds will probably also be assigned the ice phase.

Table 1 indicates that the global values of the inhomogeneity parameters for July are similar for water and ice clouds. Table 3 suggests that the same applies for January (at least for Terra). The Table 3 entries for Land/Ocean and Fig. 2 reveal that this near equality is the result of some latitudinal cancellations. In July, ice clouds tend to be more heterogeneous in the Tropics, northern subtropics and northern polar regions (where retrievals are less reliable), but there are extensive mid-latitude regions in both the Northern (NH) and Southern hemisphere (SH) where the values of χ for both types of clouds are almost identical. In contrast, January ice clouds seem to be more homogeneous than liquid clouds in most of the globe except the zone near the equator, north of 40°N, and the high latitudes of the SH (again an area of less reliable retrievals). Overall, the

latitudinal variability of χ is more pronounced for ice clouds than liquid clouds. This is probably because ice cloud morphology and mean optical properties are quite different among ice clouds associated with mid-latitude weather systems (some of which may be of mixed phase), thick cirrus anvils/deep convective towers that occur frequently in equatorial regions, and relatively thin cirrus clouds blanketing extensive regions without distinct geographic preference. Moreover, the presence of ice phase increases the chances of multi-layer cloud occurrences. It is not therefore surprising that histograms of $\hat{\chi}^C(m,n)$ for ice clouds are broader than their counterparts for liquid clouds (Fig. 3). In other words, ice clouds are more likely to be either extremely homogeneous or extremely heterogeneous compared to liquid clouds.

c. Inhomogeneity from Terra vs. inhomogeneity from Aqua

Although the full diurnal cycle cannot be resolved with the two sun-synchronous satellite platforms (Terra and Aqua) that carry MODIS, it is nevertheless instructive to examine whether there are distinct differences in cloud heterogeneity at global scales before and after local noon. Tables 3a and 3b give global, hemispheric, and land-only/ocean-only (global and hemispheric) averages of χ and ν_{MLE}, respectively, for both liquid and ice clouds and for both months. Aqua (crossing the equator at ~1:30 pm local time) has almost always smaller values of χ (larger apparent cloud heterogeneity) than Terra (with an approximate equatorial crossing time of 10:30 am), the exception being marine ice clouds. For summer ice clouds, the Terra-Aqua differences are greater over land than over ocean, probably reflecting the stronger diurnal cycle of convection over land. Figure 4 shows $\left\langle \chi^C(n) \right\rangle$ separately for Terra and Aqua. Terra liquid clouds appear more

homogeneous nearly everywhere for both months, except for northern midlatitudes, while ice clouds exhibit fewer differences in the zonal distribution of χ between the two satellites; the major divergence of values (Terra clouds more homogeneous than Aqua clouds) occurs in the SH tropics in January (an area of convective activity) and in the mid-latitudes of the NH in July (again, Terra clouds more homogeneous).

d. Winter vs. summer inhomogeneity

Table 3 and the figures shown thus far included results for both July and January, even though the contrast between these two months was not itself discussed. We will now revisit some of these results in order to concentrate on seasonal differences. The first order comparison, namely that among hemispheric averages, is captured in Table 3: for liquid clouds, winter and summer hemispheric values show seasonal symmetry, i.e., NH winter is close to SH winter and NH summer almost matches SH summer (this is better for Terra and applies even when land and ocean hemispheric values are compared separately); for ice clouds, NH winter matches SH winter, but NH summer has more inhomogeneous clouds than SH summer (this difference is less pronounced for Aqua and is driven by marine clouds for both satellite platforms). Overall, clouds are more inhomogeneous in the winter for both phases, with most of the contribution to this difference coming from marine clouds (especially for liquid clouds).

Figure 4 shows increasing liquid cloud inhomogeneity as one moves from northern to southern latitudes in July while the opposite takes place in January. The July and January values of $\langle \chi^C(n) \rangle$ meet around the Tropics, but then diverge in the mid-latitudes with July inhomogeneity being greater (smaller $\langle \chi^C(n) \rangle$ values) in the SH and January

inhomogeneity being greater in the NH. Same mid-latitude behavior can be discerned for ice clouds, but in this case there is a trough of local inhomogeneity maximum in the Tropics which highlights the contrast between the Tropics (deep convective clouds) and summer mid-latitudes (cirrus). Still, the ice clouds of winter mid-latitude storm systems (stratiform precipitating clouds that may be of mixed phase), observed under lower illuminations, appear more inhomogeneous than tropical convective clouds.

e. Day to day variability of cloud inhomogeneity

Daily global or hemispheric values of the inhomogeneity parameters can be derived from eq. (9) (and its counterparts for ν). In this subsection we highlight some aspects of the day to day variability of these values with the aid of Fig. 5 which summarizes the results in boxplot form (see caption for explanation of the information conveyed). The plot features to concentrate on is the width (distance between top and bottom) of the boxes and the distance between the endpoints of the lines extending from the top and bottom of the boxes. Both features give a quantitative assessment of the range of $\tilde{\chi}_l^C$, i.e., the larger they are the larger the day-to-day variability. Hemispheric values exhibit significantly larger day-to-day variability than global values, as expected, with the SH being in general more variable in time, regardless of whether it is winter or summer. Ice cloud inhomogeneity on global scales changes more from day to day than that for liquid clouds, complementing previous results on the width of $\widehat{\chi}^C(m,n)$ histograms. Finally, there is slight tendency of the day-to-day variability of $\tilde{\chi}_l^C$ for Terra to be smaller than that of Aqua for liquid phase clouds while the opposite occurs for ice clouds.

f. Geographical distribution of inhomogeneity

In this section we examine regional characteristics of the inhomogeneity parameters that briefly touch on the behaviour of individual cloud regimes. Only the major features are discussed here with detailed analysis of specific regions with a multi-month dataset left for a future study. Zonal distributions of χ have already been shown in previous figures (e.g., Fig. 4). In those figures it can be seen that the most inhomogeneous clouds are observed in the mid-latitudes of the winter hemispheres. Local minima in $\langle \chi^C(n) \rangle$ for liquid clouds are observed around 60° in the winter hemispheres, while for ice clouds the minimum shifts to ~45° S during the SH winter and ~55°N for during NH winter. In the vicinity of the Intertropical Convergence Zone (ITCZ), coarsely identified as the tropical local maximum in cloud fraction and τ (not shown), $\langle \chi^C(n) \rangle$ is close to 0.7 (in general agreement with the high cloud results of RDC).

Zonal analysis was also performed separately for land and ocean gridpoints (coastal gridpoints containing both ocean and land surfaces were excluded from the calculations). The much weaker inhomogeneity of continental liquid and ice clouds in the Tropics and Subtropics relative to marine clouds is reversed at mid- and high latitudes of the summer hemispheres (Fig. 6). Table 3 indicates that on global scales continental liquid clouds are less inhomogeneous than marine liquid clouds (as was found by RDC); for ice clouds this is also generally true, with the exception of summer afternoon clouds.

Plates 1 and 2 show the full geographical distribution of $\hat{\chi}^C(m,n)$ as derived from eq. (7) for Terra. These maps of $\hat{\chi}^C(m,n)$ can be compared with similar maps from ISCCP provided separately for low, middle and high clouds in http://isccp.giss.nasa.gov

even though the latter show the inhomogeneity parameter ε, which relates to χ via $\varepsilon \approx 1-\chi$ only within the range of optical thickness for which ETA works best (τ~5-30). Direct comparison of MODIS and ISCCP has also other caveats: the grid on which the parameters are evaluated (1°x1° for MODIS, ~$(280\text{km})^2$ for ISCCP) is different, and so is the pixel size of the original retrievals (1 km for MODIS, ~5 km for ISCCP), and the sampling scale (~5 km for MODIS, ~30 km for ISCCP). Other factors that distinguish the two datasets, are the different temporal sampling (sun-synchronous vs. geostationary) and the different cloud retrieval methods.

The marine stratocumulus regimes off the west coasts of N. America, S. America, and south-central Africa appear rather homogeneous in these maps with values of χ greater than ~0.85 in July and above ~0.8 in January (decreasing as one moves away from the coast), consistent with the satellite values of Pincus et al. (1999). These values are, however, larger than ~0.7 and ~0.6 found by Cahalan et al. (1994) and Cahalan et al. (1995) for FIRE (First ISCCP Regional Experiment) and ASTEX (Atlantic Stratocumulus Transition Experiment) marine boundary layer clouds, but which were based on different measurements (one or half minute-averaged microwave radiometer ground measurements) resolving temporal and not spatial (as in MODIS) variations. RDC finds annual values of ε between 0.1 and 0.2 for these cloud systems which correspond to an approximate range of 0.8-0.9 for χ. The region of active convection over Indonesia (ice cloud panels) appears to be characterized by χ values close to 0.6 (annual ε between 0.3 and 0.4 in RDC). The same value approximately applies for mid-latitude storm systems of both winter hemispheres. The ice clouds of the summer hemispheres are quite

homogeneous with values of χ above 0.8 in most regions while the annual values of ε in RDC for mid-latitude high clouds are between 0.1 and 0.2 for both hemispheres. Comparison with the ISCCP results of RDC is not straighforward only for the reasons previously mentioned, but also because of the different cloud-type classification. Still, the first-order visual ISCCP-MODIS map comparison for the two months of our analysis with corresponding seasonal results in the ISCCP website suggests a large degree of qualitative agreement.

g. Relationship between χ and cloud fraction

If cloud horizontal inhomogeneity were to be diagnosed in an LSM via an observation-based parameterization, vertical profiles of inhomogeneity would ideally be needed. This is because LSMs have vertically discretized atmospheres, and therefore, clouds. As has been noted in a prior discussion, this paper describes horizontal variations of *total* cloud optical thickness, a limitation that cannot be overcome with the present dataset. Hence, unless single layer clouds are reliably identified and the variability is assumed not to change with height (Barker et al., 1996; Oreopoulos and Barker, 1999), it would not be entirely justified to use the present dataset to develop parameterizations of cloud inhomogeneity. Nevertheless, it may still be interesting to look at the relationship between MODIS cloud inhomogeneity and cloud fraction since there have been previous efforts along this direction (Barker et al., 1996; Oreopoulos and Davies, 1998b).

If all gridpoints of a single day with liquid phase clouds are used to scatterplot χ vs. cloud fraction, at first glance there appears to be no apparent relationship. Indeed, when χ values are averaged within individual cloud fraction bins (large points in Fig. 7), mean χ

seems to remain relatively constant around 0.7 for cloud fractions up to ~0.9. However, there is a clear increase for the last two cloud fraction bins. Remarkably, the almost overcast gridpoints (bin 0.99-1 in Fig. 7) are distinctly more homogeneous (on average) than the gridpoints falling within the 0.9-0.99 bin. This general tendency was also confirmed (for both months and satellite platforms) when the analysis was restricted to the three marine stratocumulus regions off the coasts of California, Peru, and Angola (not shown) in agreement with Barker et al. (1996), but in disagreement with Cahalan et al. (1994) who found from diurnal analysis of microwave radiometer data that California marine stratocumulus during FIRE were most variable close to their cloud fraction peak. Further research is apparently needed to clarify the causes of these conflicting results and to relate them to the physical processes that generate, maintain, and destroy these clouds.

It should be pointed out that even for our current dataset the relationship between χ and cloud fraction is not unique or simple. Fig. 8 shows that it depends on cloud phase and mean optical thickness. For liquid clouds of intermediate $\bar{\tau}$ (between 10 and 20), for example, χ follows a monotonic increase with cloud fraction, while for thick clouds of both phases ($\bar{\tau} > 20$) the relationship is more complex. It would be interesting to examine whether future LSM schemes with subgrid cloud variability capabilities will be able to reproduce such behaviour for integrated τ.

5. Discussion and Conclusions

We provide the first extensive attempt to infer horizontal variability of total cloud optical thickness τ ("cloud inhomogeneity") from the MODIS instrument aboard Terra and Aqua. The climatology of cloud inhomogeneity is based on calculations of monthly

inhomogeneity parameter values at 1°x1°, zonal, and global spatial scales for two full months (January 2004 and July 2003) of MODIS Atmosphere Level-3 data. Geographical, diurnal, and seasonal changes of cloud inhomogeneity are studied separately for liquid and ice phase clouds.

Cloud inhomogeneity is found to be generally weaker in summer than in winter, weaker over land than ocean (except for afternoon summer ice clouds), weaker in general for local morning (Terra) than local afternoon (Aqua), similar for liquid and ice clouds on a global scale (especially for morning clouds), but with larger temporal and spatial variations for ice clouds. It is also relatively insensitive to whether water path or τ distributions are used. Day to day variability of hemispheric values is stronger for ice clouds and for the Southern Hemisphere. Monthly values at hemispherical scales of the inhomogeneity parameter ν (roughly the square of the ratio of τ mean to standard deviation) vary widely from ~1.7 (mean MLE value of marine afternoon liquid clouds during the NH winter) to ~4 (mean MLE value for continental morning ice clouds during SH winter), while for the inhomogeneity parameter χ (the ratio of the logarithmic to linear mean), which is the centerpiece of our presentation, from ~0.65 to 0.8. Zonal monthly values of χ below 0.6 are possible while monthly values of individual gridpoints occasionally assume values below 0.5. Variability of τ is not clearly related to cloud fraction (except perhaps for liquid clouds of intermediate τ), but for overcast or near overcast regions of both phases there is a tendency for clouds to be more homogeneous. This needs further investigation in view of the expectation that overcast scenes will be less affected by 3D effects than broken cloud scenes. Finally, there is broad agreement in

geographical distributions of MODIS and ISCCP inhomogeneity despite inherent differences in cloud retrieval and parameter calculation methods.

We have demonstrated that analysis of MODIS Level-3 data reveals interesting aspects of the climatology of cloud horizontal inhomogeneity and can be used for validation of LSM schemes that are able to predict subgrid cloud variability (e.g., Tompkins, 2002). The MODIS retrievals, are of course, subject to the limitations of plane-parallel retrievals, but the impact of neglecting cloud 3D radiative effects cannot be easily investigated with the current dataset. Low solar illuminations increase cloud variability as perceived by plane-parallel retrievals (e.g., Oreopoulos et al., 2000), making winter clouds appear more heterogeneous than summer clouds even if the cloud fields themselves remained unchanged. Separating actual from perceived changes of cloud inhomogeneity remains an open issue to be perhaps addressed with new aggregation strategies of Level-2 MODIS retrievals. The nature of sun-synchronous satellite orbits, however, undermines such efforts by convolving solar geometry, latitude, seasonal, and cloud type dependencies. Future studies examining systematic cloud retrieval dependencies on view angle may therefore be more illuminating.

The non-linear dependence of solar and longwave radiation on cloud optical properties has to be taken into account for accurate calculations of the radiative energy budget. The present work, along with that by Rossow et al. (2002), has reaffirmed that sufficient observations currently exist to achieve this. One possible approach is to provide Column Radiation Models with cloud inhomogeneity information from MODIS along with vertical variability from Cloud Resolving Models or future CloudSat retrievals (Stephens et al., 2002). We hope to perform such a study in the future.

Acknowledgements: The financial support of NASA under grants NAG5-11631 and 621-30-86, and of DoE's ARM program under grant DE-AI02-00ER62939 is gratefully acknowledged. We would like to thank Steve Platnick for his invaluable assistance in understanding various aspects of the MODIS cloud products. Also thanks go to Paul Hubanks and Bill Ridgway for their help with software and other technical issues. The comments of an anonymous reviewer helped clarify and improve many aspects of the analysis.

References

Barker, H. W., 1996: A parameterization for computing grid-averaged solar fluxes for inhomogeneous marine boundary layer clouds, part I: methodology and homogeneous biases. *J. Atmos. Sci.*, **53**, 2289-2303.

Barker, H. W., B. A. Wielicki, L. Parker, 1996: A parameterization for computing grid-averaged solar fluxes for inhomogeneous marine boundary layer clouds, part II: validation using satellite data. *J. Atmos. Sci.*, **53**, 2304-2316.

Cahalan, R. F., W. Ridgway, W. J. Wiscombe, T. L. Bell and J. B. Snider, 1994: The albedo of fractal stratocumulus clouds. *J. Atmos. Sci.*, **51,** 2434-2455.

Cahalan, R. F., D. Silberstein, and J. B. Snider, 1995: Liquid water path and plane-parallel albedo bias during ASTEX. *J. Atmos. Sci.*, **52,** 3002-3012.

Harshvardhan, and D. A. Randall, 1985: comments on "The parameterization of radiation for numerical weather prediction and climate models". *Mon. Wea. Rev.*, **113,** 1832-1833.

Jakob, C. and S. A. Klein, 1999: The role of vertically varying cloud fraction in the parameterization of microphysical processes in the ECMWF model. *Q. J. R. Meteorol. Soc.*, **125**, 941-965.

King, M. D., W. P. Menzel, Y. J. Kaufman, D. Tanré, B.-C. Gao, S. Platnick, S. A. Ackerman, L. A. Remer, R. Pincus, and P. A. Hubanks, 2003: Cloud and aerosol properties, precipitable water, and profiles of temperature and water vapor from MODIS. *IEEE Trans. Geosc. Rem. Sens.*, **41**, 442-458.

Oreopoulos, L., and R. Davies, 1998a: Plane parallel albedo biases from satellite observations. Part I: Dependence on resolution and other factors. *J. Climate*, **11**, 919-932.

Oreopoulos, L., and R. Davies, 1998b: Plane parallel albedo biases from satellite observations. Part II: Parameterizations for bias removal. *J. Climate*, **11**, 933-944.

Oreopoulos, L., and H. W. Barker, 1999: Accounting for subgrid-scale cloud variability in a multi-layer 1d solar radiative transfer algorithm. *Q. J. Roy. Met. Soc.,* **126,** 301-330.

Oreopoulos, L., R. F. Cahalan, A. Marshak, and G. Wen, 2000: A new normalized difference cloud retrieval technique applied to Landsat radiances over the Oklahoma ARM site. *J. Appl. Meteor.*, **39**, 2305-2321.

Oreopoulos, L., M.-D. Chou, M. Khairoutdinov, H. W. Barker, and R. F. Cahalan, 2004: Performance of Goddard Earth Observing System GCM Column Radiation Models under heterogeneous cloud conditions. *Atmos. Res.*, **72**, 365-382.

Oreopoulos, L., 2005: The impact of subsampling on MODIS Level-3 statistics of cloud optical thickness and effective radius, *IEEE Trans. Geosc. Rem. Sens.*, **43**, 366-373.

Pincus, R., S. A. McFarlane, and S. A. Klein, 1999: Albedo bias and the horizontal variability of clouds in subtropical marine boundary layers: observations from ships and satellites. *J. Geophys. Res.*, **104**, 6183-6191.

Platnick, S., 2000: Vertical photon transport in cloud remote sensing problems. *J. Geophys. Res.*, **105**, 22,919-22,935.

Platnick, S., M. D. King, S. A. Ackerman, W. P. Menzel, B. A. Baum, , J. C. Riédi, and R. A. Frey, 2003: The MODIS cloud products: Algorithms and examples from Terra. *IEEE Trans. Geosc. Rem. Sens.*, **41**, 459-473.

Räisänen, P., G. Isaac, H. W. Barker, and I. Gultepe, 2003: Solar radiative transfer for stratiform clouds with horizontal variations in liquid-water path and droplet effective radius. *Q. J. R. Meteor. Soc.*, **129**, 2135-2149.

Räisänen, P., H. W. Barker, M. F. Khairoutdinov, J. Li, and D. A. Randall, 2004: Stochastic generation of subgrid-scale cloudy columns for large-scale models. *Q. J. R. Meteor. Soc.*, in press.

Rossow, W. B., C. Delo, and B. Cairns, 2002: Implications of the observed mesoscale variations of clouds for the Earth's radiation budget. *J. Climate*, **15**, 557-585.

Stephens, G. L., and coauthors, 2002: The CloudSat mission and the A-train. *Bull. Amer. Meteor. Soc.*, **83,** 1771-1790.

Tompkins, A. M., 2002: A prognostic parameterization for the subgrid-scale variability of water vapor and clouds in large-scale models and its use to diagnose cloud cover. *J. Atmos. Sci.,* **59,** 1917–1942.

Wilks, D. S., 1995: *Statistical Methods in the Atmospheric Sciences*, Academic Press. 467pp.

Table 1

	Liquid					Ice				
	τ_1	τ_2	τ_1 QA	W_1	W_2	τ_1	τ_2	τ_1 QA	W_1	W_2
χ	0.745	0.742	0.771	N/A	0.731	0.735	0.735	0.780	N/A	0.747
$\nu_{\mathbf{MLE}}$	2.87	2.76	3.19	N/A	2.66	2.91	2.89	3.40	N/A	2.85
$\nu_{\mathbf{MOM}}$	2.62	2.55	2.96	2.63	2.37	2.71	2.69	3.09	3.00	2.61

Table 2

χ	ν_{MLE} (liq)	ν_{MOM} (liq)	ν_{MLE} (ice)	ν_{MOM} (ice)
0.50	1.06	0.87	1.03	0.82
0.55	1.29	1.09	1.28	1.05
0.60	1.58	1.35	1.59	1.34
0.65	1.93	1.69	1.98	1.72
0.70	2.36	2.10	2.46	2.21
0.75	2.89	2.62	3.05	2.83
0.80	3.53	3.27	3.79	3.63
0.85	4.32	4.08	4.71	4.65
0.90	5.27	5.09	5.84	5.96
0.95	6.45	6.34	7.26	7.64

Table 3a

	TERRA				AQUA			
	January		*July*		*January*		*July*	
	Liquid	*Ice*	*Liquid*	*Ice*	*Liquid*	*Ice*	*Liquid*	*Ice*
GLOBAL	0.748	0.748	0.745	0.735	0.711	0.739	0.710	0.737
NH	0.716	0.710	0.786	0.757	0.682	0.707	0.759	0.753
SH	0.774	0.784	0.700	0.709	0.736	0.770	0.658	0.718
LAND	0.788	0.748	0.796	0.798	0.750	0.716	0.759	0.748
OCEAN	0.736	0.750	0.727	0.716	0.700	0.750	0.694	0.735
NH LAND	0.776	0.721	0.793	0.793	0.754	0.717	0.763	0.740
NH OCEAN	0.680	0.704	0.782	0.739	0.640	0.701	0.756	0.760
SH LAND	0.802	0.795	0.796	0.802	0.735	0.709	0.739	0.768
SH OCEAN	0.768	0.781	0.685	0.697	0.736	0.782	0.645	0.711

Table 3b

	TERRA				AQUA			
	January		*July*		*January*		*July*	
	Liquid	*Ice*	*Liquid*	*Ice*	*Liquid*	*Ice*	*Liquid*	*Ice*
GLOBAL	2.96	3.18	2.87	2.91	2.58	3.09	2.57	2.87
NH	2.64	2.64	3.35	3.21	2.34	2.60	3.10	3.11
SH	3.23	3.68	2.34	2.54	2.79	3.54	1.99	2.58
LAND	3.66	3.34	3.39	3.70	3.16	2.90	2.95	3.00
OCEAN	2.76	3.15	2.70	2.68	2.41	3.19	2.45	2.84
NH LAND	3.70	3.15	3.31	3.53	3.37	3.02	3.00	2.83
NH OCEAN	2.00	2.33	3.38	3.05	1.73	2.35	3.15	3.25
SH LAND	3.42	3.60	3.46	4.07	2.63	2.55	2.71	3.48
SH OCEAN	3.19	3.69	2.16	2.34	2.82	3.74	1.88	2.46

Table captions

Table 1 Comparison of different methods to obtain global inhomogeneity parameters for Terra July 2003 data. The subscript "1" refers to using the SDS moments, and the subscript "2" to using the histogram SDS; "τ" is for optical thickness-based parameters and "W" for water path-based parameters; QA refers to QA-weighted optical thickness moments (see text). No moment-based estimates of the inhomogeneity parameters χ and ν_{MLE} can be obtained for W since there is no $\overline{\ln W}$ SDS.

Table 2 Conversion guide between $\langle \chi^C \rangle$ and $\langle \nu^C_{MLE} \rangle$ and $\langle \nu^C_{MOM} \rangle$ derived from Terra July 2003 and January 2004 data.

Table 3a Summary of monthly global (or hemispheric) inhomogeneity parameter χ values as derived from eq. (10).

Table 3b As in Table 3a, but for ν_{MLE}.

Figure captions

Figure 1 $\langle \chi^C(n) \rangle$ from eq. (8) for liquid (top) and ice (bottom) clouds as inferred from Terra τ and W histogram SDSs for January 2004 and July 2003.

Figure 2 $\langle \chi^C(n) \rangle$ from eq. (8) for liquid and ice phase clouds as inferred from Terra τ SDS moments. Top panel is for January 2004 and bottom panel for July 2003.

Figure 3. Comparison of liquid and ice phase histograms of the monthly values of χ derived from eq. (7) for Terra. Top panel is for January 2004 and bottom panel for July 2003.

Figure 4 $\langle \chi^C(n) \rangle$ from eq. (8) for Terra and Aqua. Top panel is for liquid clouds and bottom panel is for ice clouds.

Figure 5. Box plots summarizing the day to day variability of $\tilde{\chi}_l^C$ as derived from the 31 daily values estimated using eq. (9). Each box encloses 50% of the data with the median value of the variable displayed as a line. The top and bottom of the box mark the limits of ±25% of the population. The lines extending from the top and bottom of each box ("whiskers") mark the minimum and maximum global or hemispheric values of χ that fall within an acceptable range. Outliers–defined as values greater (smaller) than the upper (lower) quartile value plus (minus) 1.5 times the interquartile distance, are displayed with a small circle symbol. The top panel is for liquid clouds and the bottom panel for ice clouds. The plain white boxes are for January 2004 and the gray boxes for July 2003 (also separated by the vertical dashed line). The first box of each 3-box group is for the entire globe, the second for the NH only, and the third for the SH only (see, for

example, the first box group of the bottom panel). The solid line in the middle of each plot separates Terra and Aqua results.

Figure 6 $\left\langle \chi^C(n) \right\rangle$ from eq. (8) for Terra, calculated separately for land and ocean for both phases and both months.

Figure 7 Inhomogeneity parameter $\chi_1(m,n)$ vs. cloud fraction $C_1(m,n)$ for July 1st, 2003, liquid phase clouds from Terra observations. Only gridpoints for which the ice phase cloud fraction is less than 0.05 were included in the plot. The large symbols represent averages for 0.1-wide cloud fraction bins, except the last two which are for the 0.9-0.99 and 0.99-1 bins.

Figure 8 Ensemble mean χ from July 2003 Terra data for all 1°x1° gridpoints with clouds of one of three ranges of mean optical thickness and cloud fractions falling within the bins shown in the abscissa. Only gridpoints where the cloud fraction of the other phase is less than 0.05 are considered. "Thin" means gridpoint mean optical thickness less than 10, "intermediate" between 10 and 20, and "thick" greater than 20. Top panel is for liquid clouds, and bottom panel is for ice clouds.

Plate 1 Geographical distribution of $\widehat{\chi}^C(m,n)$ calculated from eq. (7) for liquid clouds. Top panel is for Terra January 2004, and bottom panel is for Terra July 2003.

Plate 2 As in Plate 1, but for ice clouds.

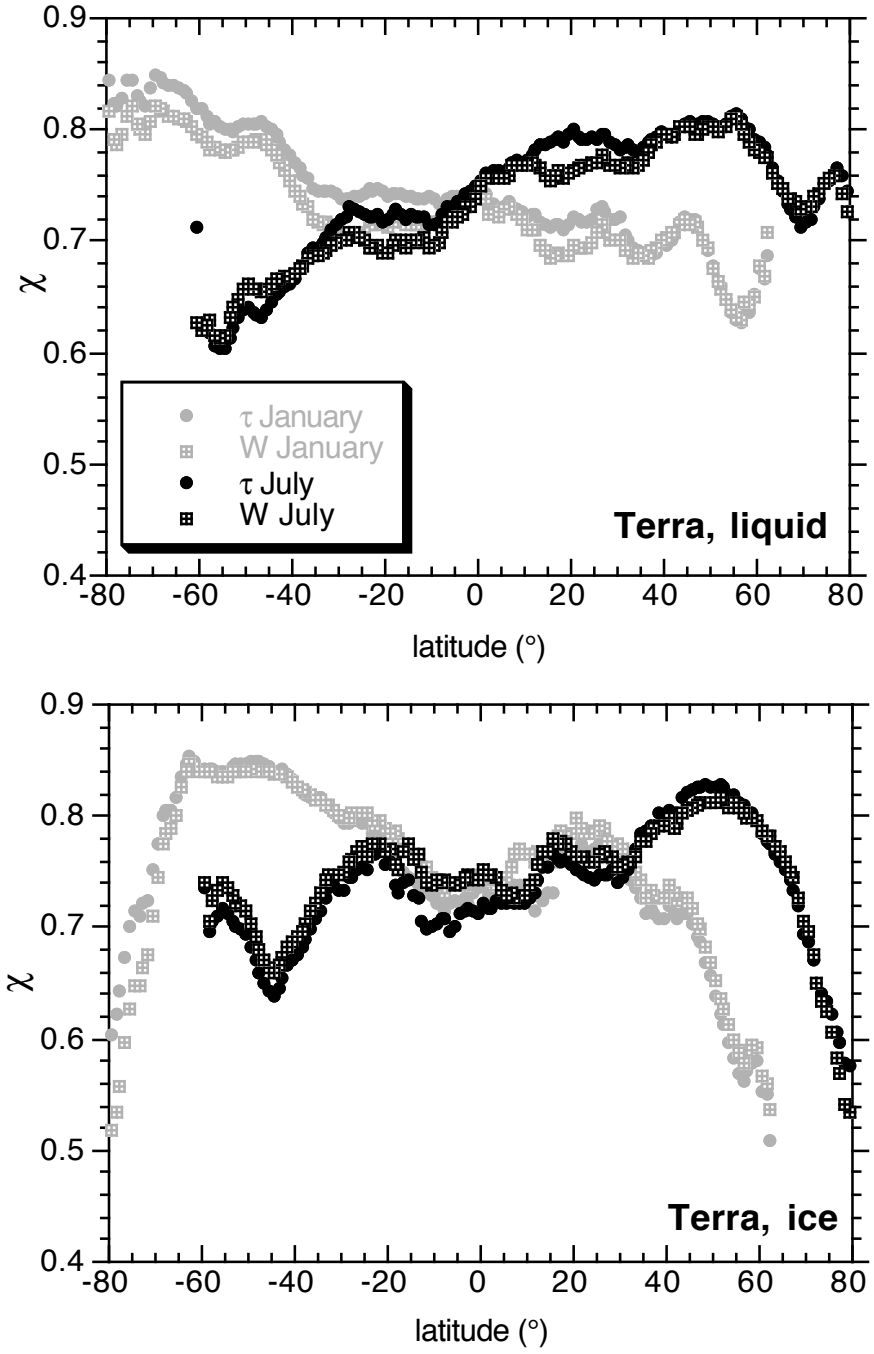
0.9
0.8
0.7
0.6
0.5
0.4
χ
τ January
W January
τ July
W July
Terra, liquid
-80
-60
-40
-20
0
20
40
60
80
latitude (°)
0.9
0.8
0.7
0.6
0.5
0.4
χ
Terra, ice
-80
-60
-40
-20
0
20
40
60
80
latitude (°)

Figure 1

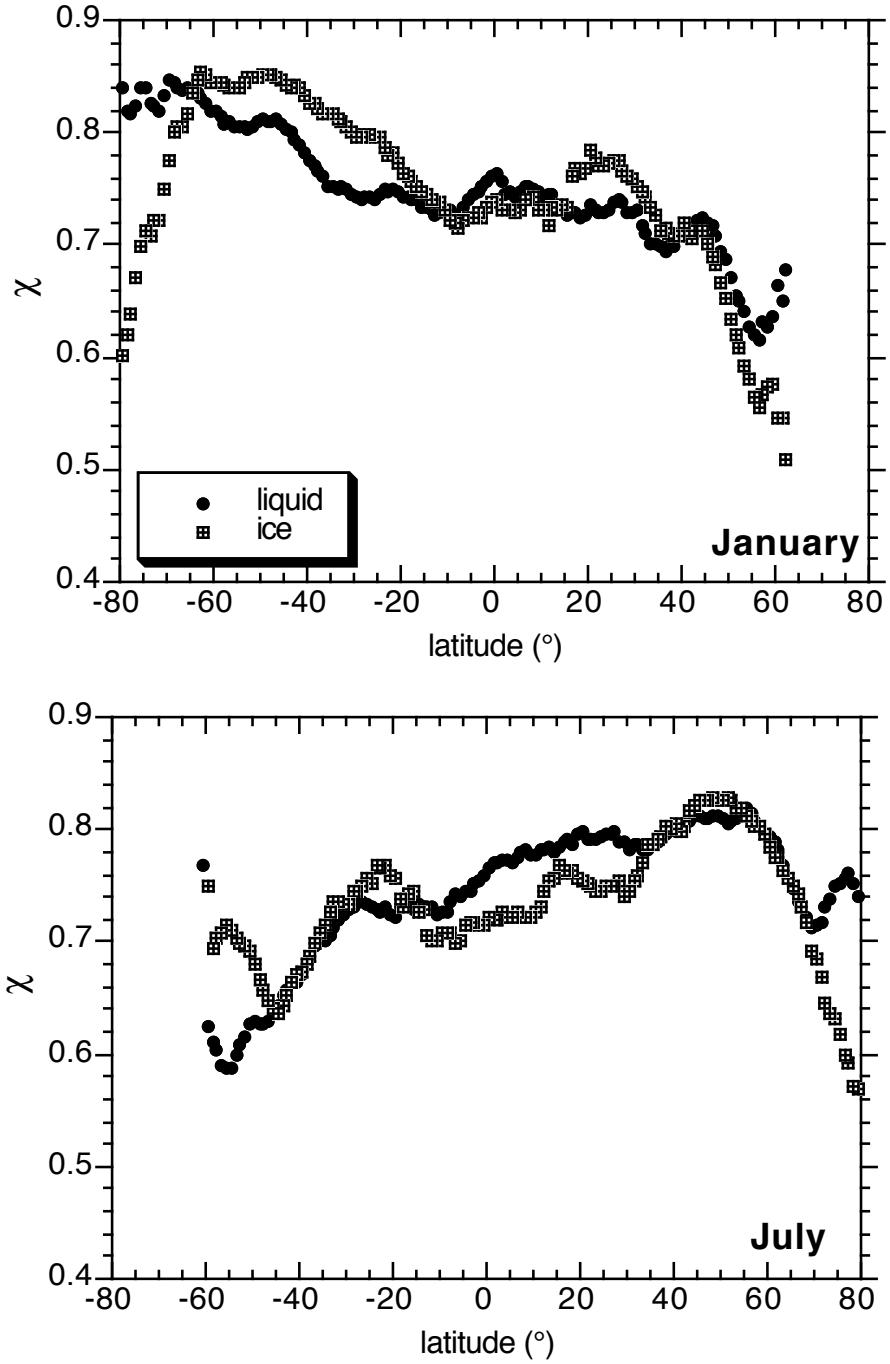
0.9
0.8
0.7
0.6
0.5
0.4
χ
liquid
ice
January
-80
-60
-40
-20
0
20
40
60
80
latitude (°)
July

Figure 2

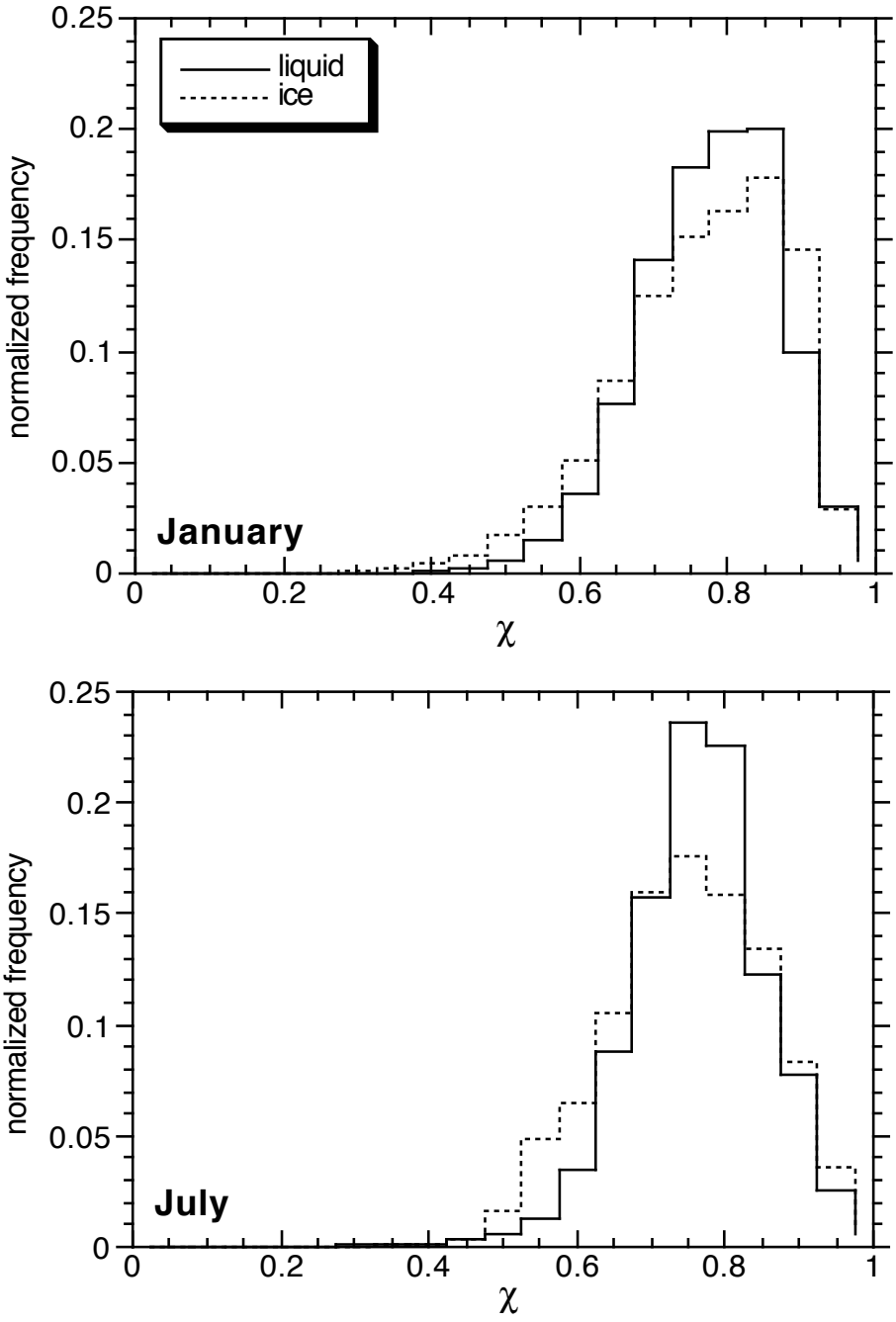
liquid
ice
January
July
normalized frequency
χ
0.25
0.2
0.15
0.1
0.05
0
0.2
0.4
0.6
0.8
1

Figure 3

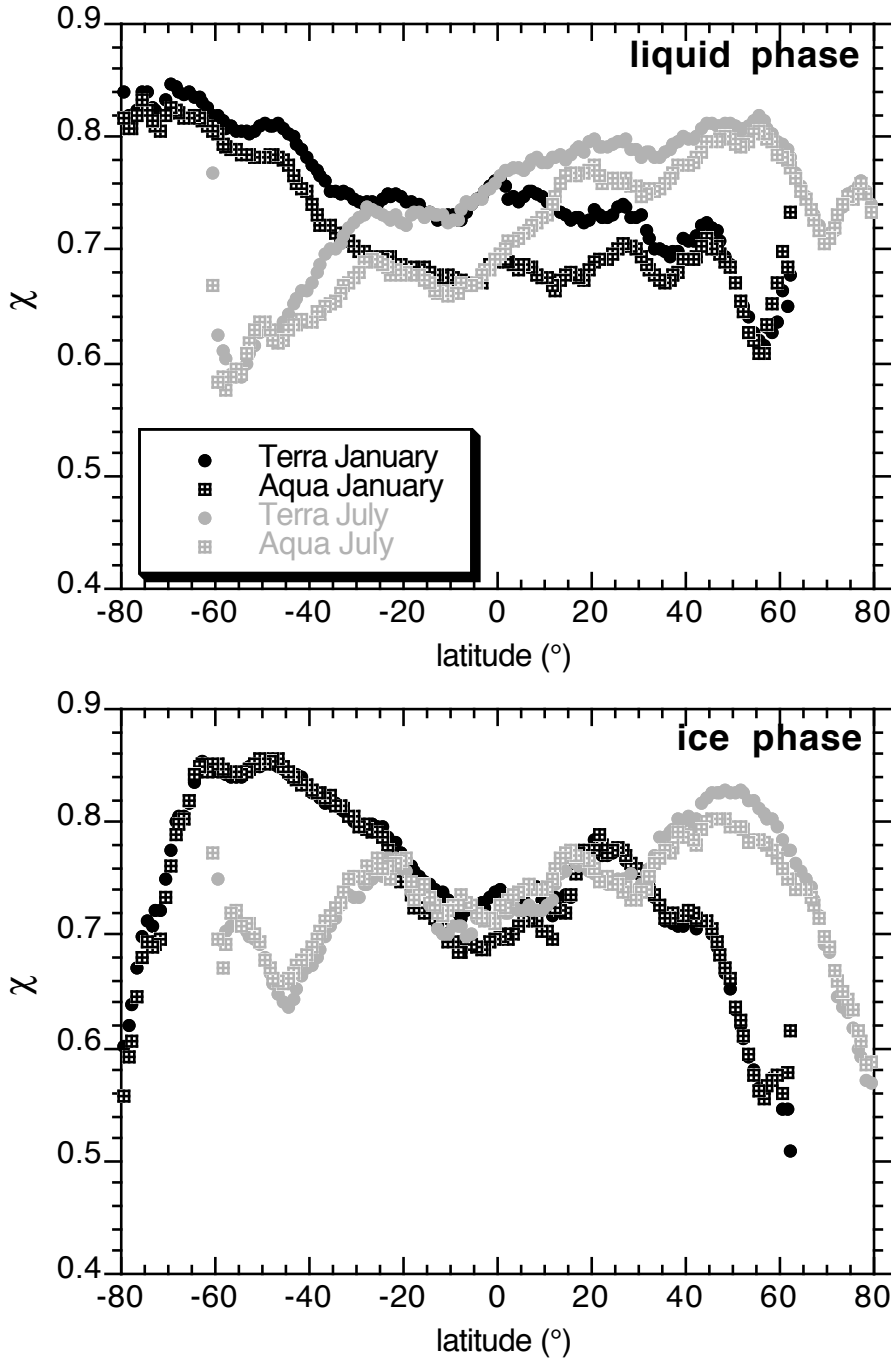
liquid phase
ice phase
Terra January
Aqua January
Terra July
Aqua July
χ
latitude (°)
0.9
0.8
0.7
0.6
0.5
0.4
-80
-60
-40
-20
0
20
40
60
80

Figure 4

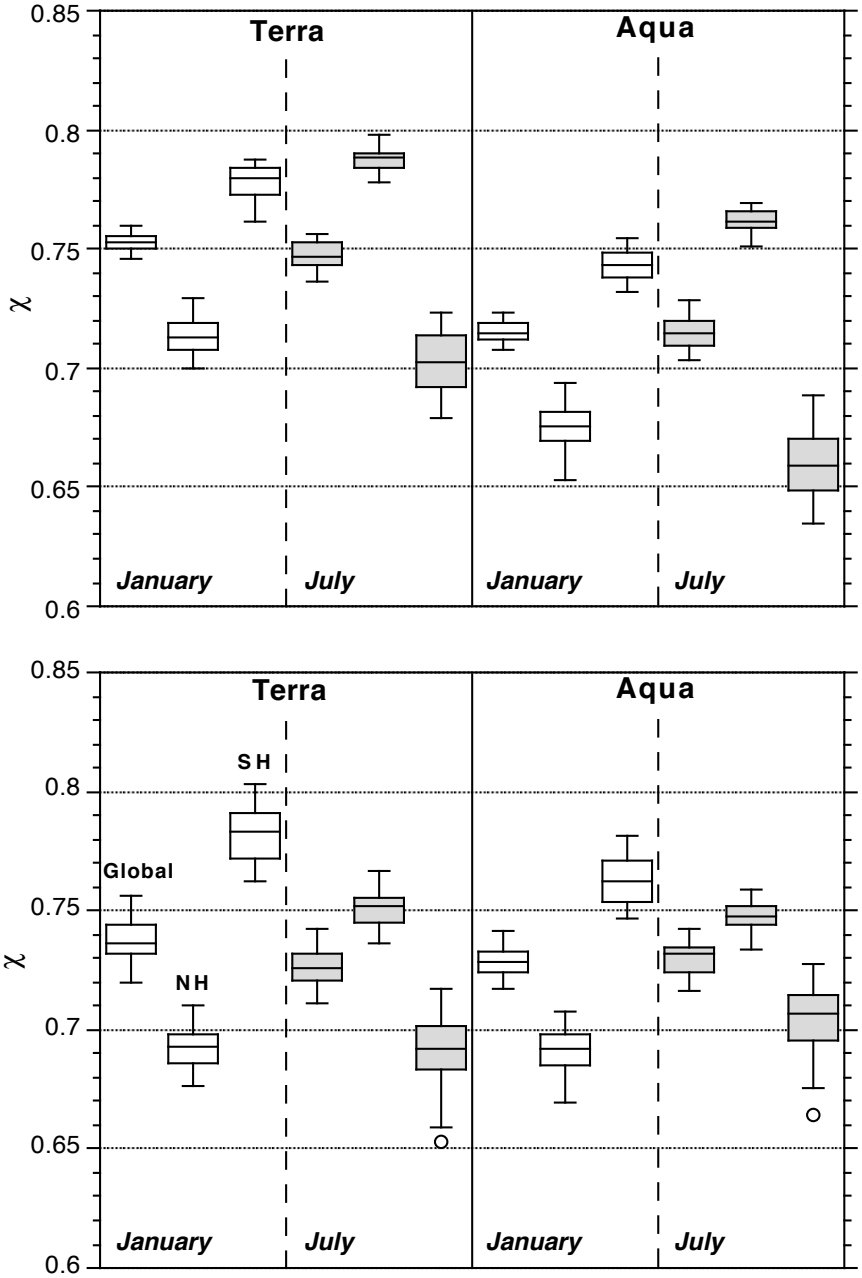
Terra
Aqua
χ
0.85
0.8
0.75
0.7
0.65
0.6
January
July
January
July
Terra
Aqua
SH
Global
NH
χ
0.85
0.8
0.75
0.7
0.65
0.6
January
July
January
July

Figure 5

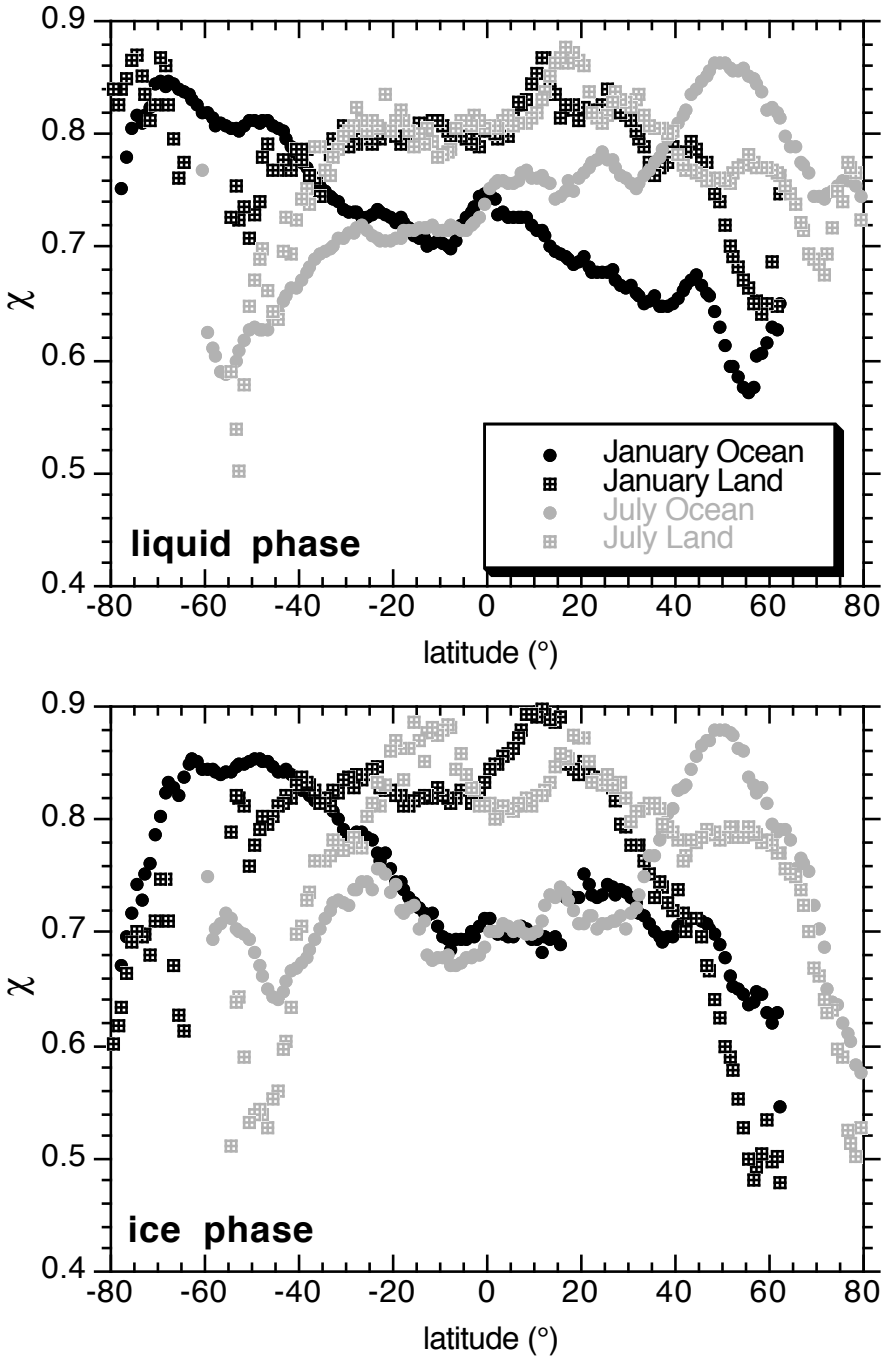
0.9
0.8
0.7
0.6
0.5
0.4
χ
January Ocean
January Land
July Ocean
July Land
liquid phase
-80
-60
-40
-20
0
20
40
60
80
latitude (°)
ice phase

Figure 6

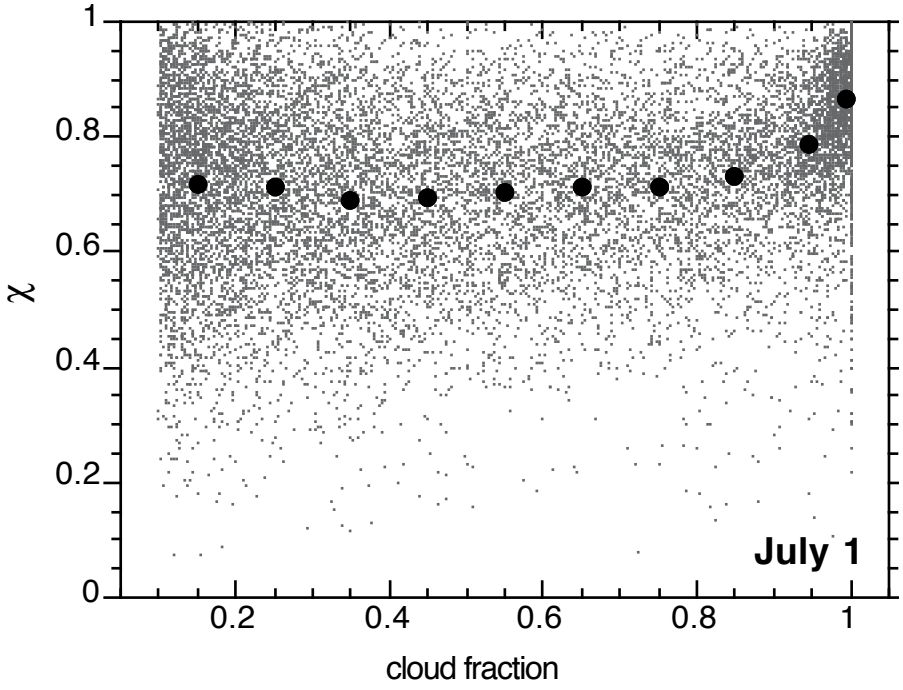

Figure 7

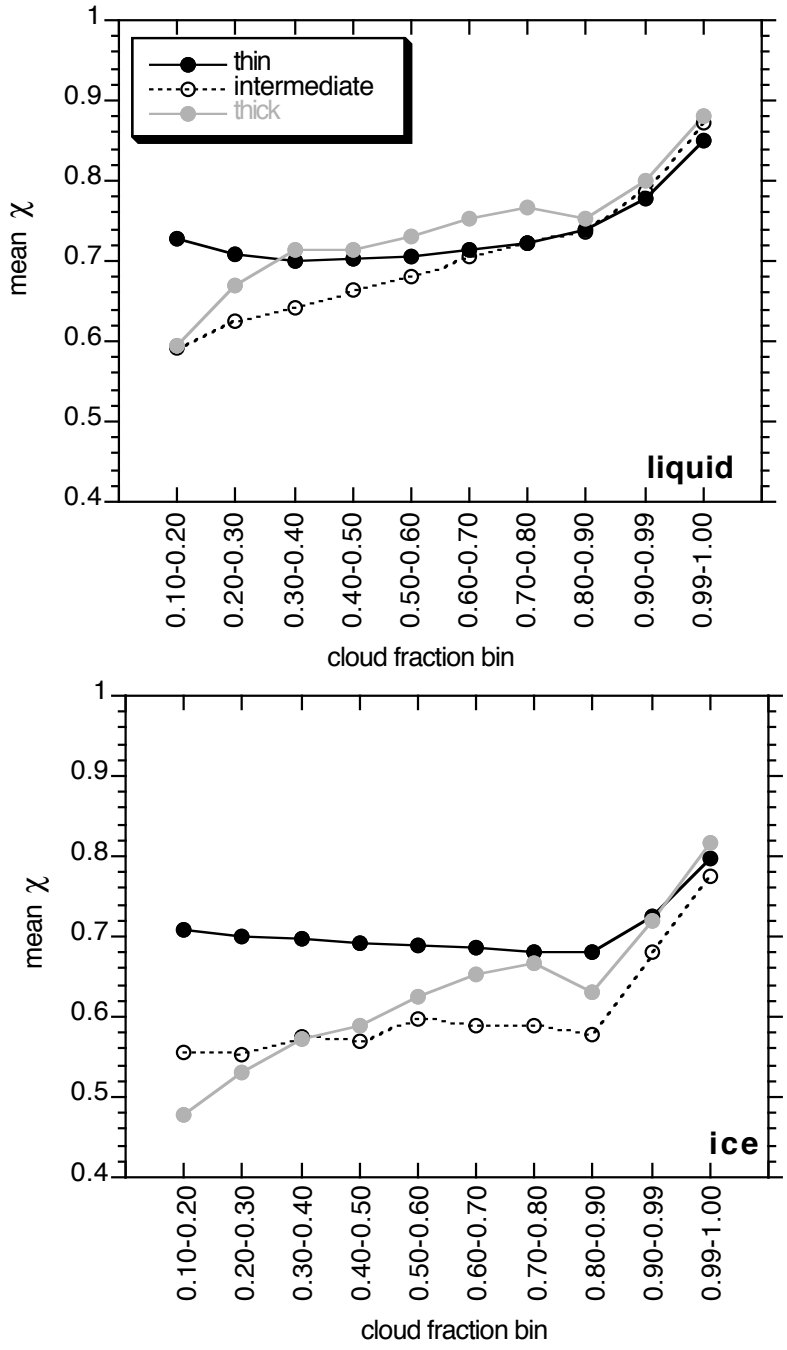
thin
intermediate
thick
liquid
ice
mean χ
cloud fraction bin
0.10-0.20
0.20-0.30
0.30-0.40
0.40-0.50
0.50-0.60
0.60-0.70
0.70-0.80
0.80-0.90
0.90-0.99
0.99-1.00
1
0.9
0.8
0.7
0.6
0.5
0.4

Figure 8

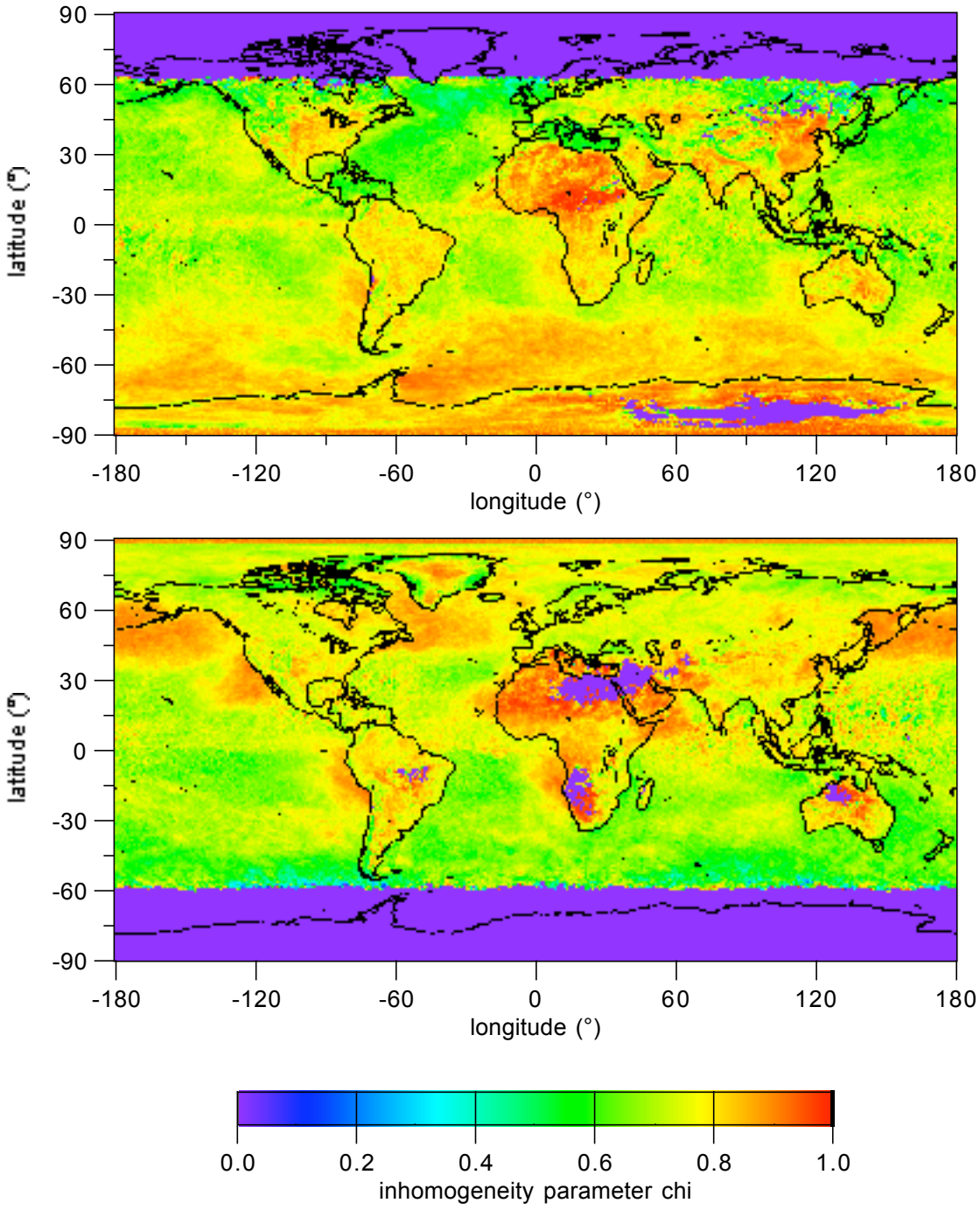
90
60
30
0
-30
-60
-90
latitude (°)
-180
-120
-60
0
60
120
180
longitude (°)
0.0
0.2
0.4
0.6
0.8
1.0
inhomogeneity parameter chi

Plate 1

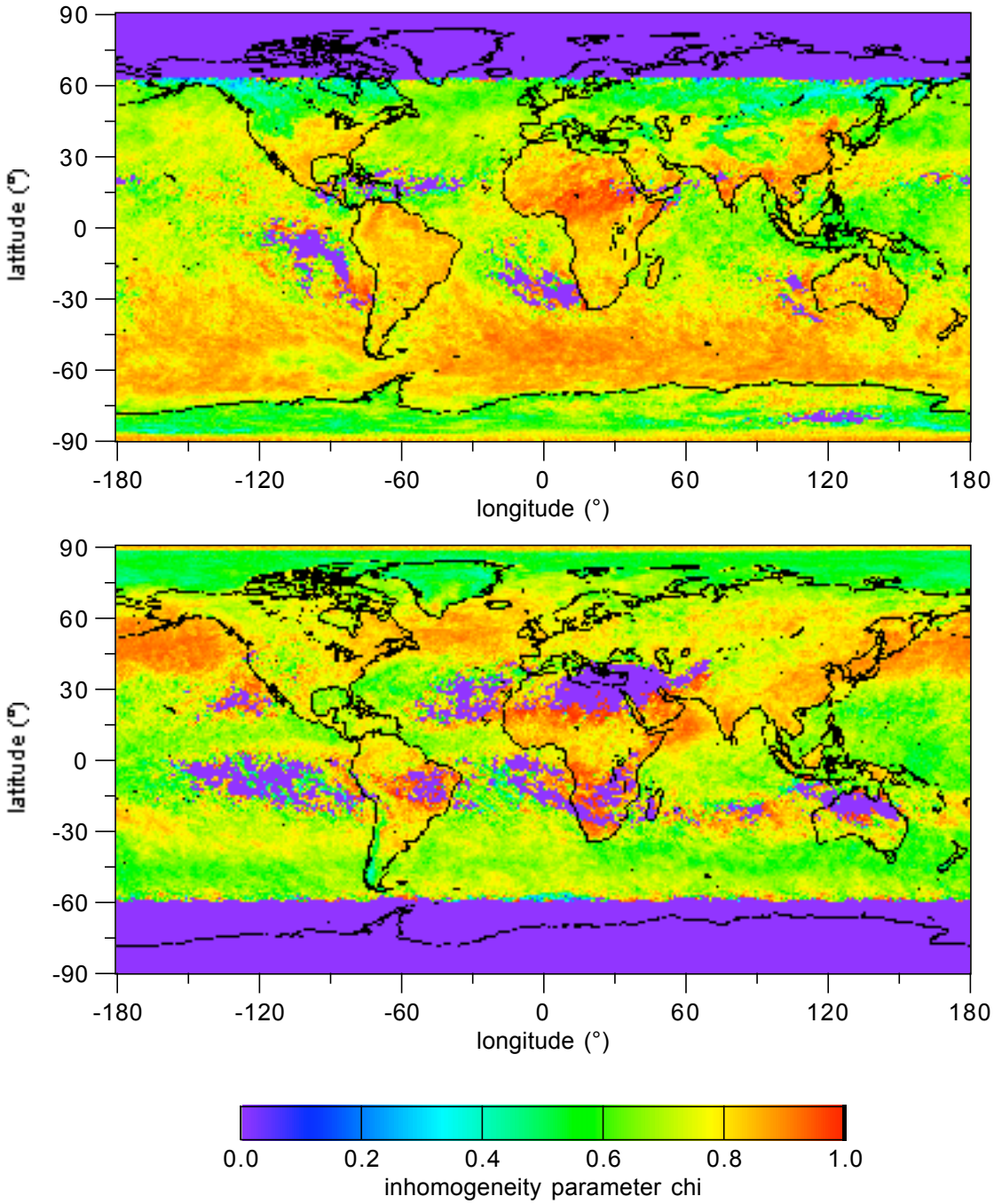
90
60
30
0
-30
-60
-90
latitude (°)
-180
-120
-60
0
60
120
180
longitude (°)
0.0
0.2
0.4
0.6
0.8
1.0
inhomogeneity parameter chi

Plate 2